NJC

Accepted Manuscript

This is an *Accepted Manuscript*, which has been through the Royal Society of Chemistry peer review process and has been accepted for publication.

Accepted Manuscripts are published online shortly after acceptance, before technical editing, formatting and proof reading. Using this free service, authors can make their results available to the community, in citable form, before we publish the edited article. We will replace this *Accepted Manuscript* with the edited and formatted *Advance Article* as soon as it is available.

You can find more information about *Accepted Manuscripts* in the Information for Authors.

Please note that technical editing may introduce minor changes to the text and/or graphics, which may alter content. The journal's standard Terms & Conditions and the Ethical guidelines still apply. In no event shall the Royal Society of Chemistry be held responsible for any errors or omissions in this *Accepted Manuscript* or any consequences arising from the use of any information it contains.

ROYAL SOCIETY OF CHEMISTRY

www.rsc.org/njc

Journal Name

ARTICLE

Low temperature operating gas sensor with high response to NO_2 based on ordered mesoporous Ni-doped In_2O_3

Received 00th January 20xx,
Accepted 00th January 20xx

DOI: 10.1039/x0xx00000x

www.rsc.org/

Qiuyue Yang,[a] Xiaobiao Cui,[a] Jiangyang Liu,[a] Jing Zhao,[b] Yinglin Wang[a] Yuan Gao,*[a] Peng Sun,[a] Jian Ma,*[a] Geyu Lu[a]

The ordered mesoporous Ni-doped In_2O_3 and undoped In_2O_3 nanostructures have been synthesized via nanocasting method which is an easy, repeatable and friendly route. The structure of the as-prepared product was characterized by X-ray diffraction(XRD), transmission electron microscopy(TEM), X-ray photoelectron spectroscopy(XPS), nitrogen physisorption and scanning electron microscopy(SEM). The results of XRD and TEM revealed the ordered structure of undoped and Ni-doped In_2O_3. The wide-angle XRD of the samples revealed that Ni incorporation may lead to lattice deformation without destroying the original crystal structure. Gas sensors based on undoped and Ni-doped In_2O_3 were fabricated and their gas sensing properties were tested. The Ni-doped In_2O_3 based sensor showed excellent selectivity toward NO_2 at the operating temperature of 58°C and the detection limit was 10 ppb. The response of the sensor based on mesoporous Ni-doped In_2O_3 was nearly 4 times higher than that of the sensor based on mesoporous undoped In_2O_3.

Introduction

Nitrogen dioxide is a kind of typical pollution gas generated from combustion chemical plants and automotive emissions. It causes acid rain, photochemical smog and ground-level ozone, which are potentially harmful to the environment. Because of this, detecting NO_2 becomes an important task for monitoring environmental pollution. Various types of techniques[1-3] have been developed to detect NO_2. Among them, gas sensors based on metal oxide semiconductor(MOS) such as In_2O_3,[4-6] SnO_2,[7] ZnO,[8] and WO_3[9] are widely used in the field of gas sensing owing to miniaturization, easy fabrication, low cost, and good long-term stability.[8,10,11] As we know, the mechanism is based on the interaction between the surface and gas molecules.[3] In the case of n-type semiconductor oxides, an electron-depleted surface layer has formed due to electron transferring from the grain surfaces to the adsorbates. Gas molecules are adsorbed and interact with oxygen adsorbates and electron on the surface, which results in the change of the depth of electron-depleted surface layer so that semiconductor sensors detect gas via variations in their resistances (or conductances).[12] So the morphology and structure play a vital role in sensing properties. Compared to bulk materials and compact films, loose and porous materials have much higher specific surface area, which improves the potential applications in gas sensing. A large amount of research on improving the sensing performance of metal oxide semiconductors by manipulating their structure morphology[6, 8, 10, 11, 13, 14] has been reported. Specially, the nanocasting method to synthesis ordered mesoporous metal oxides with hard templates has provided a facile approach to the gas sensors with optimized properties. Because of high specific surface area and ordered topological architecture, ordered mesoporous metal oxides can offer more active sites for gas adsorption and better permeability for gas diffusion.

In_2O_3 is a kind of n-type semiconductor oxides with wide band gap (E g = 3.55–3.75 eV). It is widely used in many fields such as gas sensing,[4, 14-16] UV detection,[17] dye-sensitized solar cells[16] and so on. As a promising semiconductor material for gas sensors, In_2O_3 has been extensively applied in detecting NO_2,[18] O_3,[19] CO,[4] etc. In recent years, the studies about gas sensors based on transition metals doped In_2O_3[20-24] have been reported. For instance, the dopants of Fe, Ni have been known to improve the sensing properties of In_2O_3 to specific gases.[23,24] However, the research about ordered mesoporous transition metals doped In_2O_3 for gas sensing has rarely been reported.

In this paper, ordered mesoporous Ni-doped In_2O_3 was prepared via the nanocasting route by using SBA-15 mesoporous silica as a hard template with indium and nickel nitrate salts as precursors. The morphological and structure of the material were analyzed. The sensing properties of

[a] State Key Laboratory on Integrated Optoelectronics, College of Electronic Science and Engineering, Jilin University, 2699 Qianjin Street, Changchun 130012, China.
[b] College of Electrical and Electronic Engineering, Changchun University of Technology, Changchun 130012, China

† Samples were characterized by X-ray diffraction (Rigaku D/MAX-2550 diffractometer, Cu-Kα radiation), nitrogen physisorption(Micromeritics Gemini VII surface area and porosity system at 77 K; samples degassed at 120 °C for 15 h), transmission electron microscopy (JEOL TEM-3010 instrument at an acceleration voltage of 200 kV) .The specific surface area was computed with the five point Brunauer–Emmett–Teller (BET) method and the pore size distribution was obtained from the adsorption branch of the isotherms using the Barrett–Joyner–Halenda (BJH) analysis. Analysis of the X-ray photoelectron spectroscopy (XPS) was performed on Thermo ESCALAB 250 spectrometer.
DOI: 10.1039/x0xx00000x

mesoporous In_2O_3 and Ni-doped In_2O_3 samples for NO_2 were measured. Usually, the NO_2 gas was sensed at elevated temperature [25-27]. The NO_2 sensors with high sensitivity at low operating temperature(100°C) were prepared by doping, tuning nanostructure and electrode patterns[28-31]. The major contribution of this study is to improve the sensibility, detection limit, and operation temperature of gas sensors. The Ni-doped In_2O_3 based sensor showed excellent selectivity toward NO_2 at the operating temperature of 58 °C, and the detection limit was 10 ppb.

Experimental

Synthesis of SBA-15 and In_2O_3

According to previous literature,[20] SBA-15 was synthesis as follows: 2g of Pluronic P123 ($EO_{20}PO_{70}EO_{20}$,MW = 5800, Sigma–Aldrich) was dissolved in 60 mL of HCl solution(2 mol/L) and stirring at 40°C for 2 h. After 4.25 g of tetraethylorthosilicate (TEOS) was added into the above solution, the mixture kept stirring continuously at 40°C for another 24 h, and then the resulted gel was transferred into a closed Teflon-lined stainless steel autoclave and it was heated at 100°C for 24 h. Finally, the solid product was centrifuged, washed with deionized water, dried, and sintered at 650°C for 6 h.

Mesoporous In_2O_3 was synthesized with the method of nanocasting utilizing mesoporous SBA-15 silica as a template. Typically, 1.72 g of $In(NO_3)_3{\cdot}4.5H_2O$ and 0.0172 g $Ni(NO_3)_2{\cdot}6H_2O$ were dissolved in 10 mL of absolute ethanol and stirring for 40 min to form a homogeneous solution which was served as a precursor solution. Then, 0.5 g of SBA-15 was added to the precursor solution. The mixture was stirring at 40°C till all the ethanol was evaporated, dried at 60°C and sintered at 300°C for 3 h. For higher loading, the above procedure was repeated under the same condition except that the mass of precursor was reduced by half. Sequentially, the resultant powder was sintered at 500°C for 3 h. After the silica template was removed by excess solution of NaOH (2 mol/L), the obtained material was centrifuged, washed several times and dried for 6 h. Similarly, mesoporous pure In_2O_3 was synthesized by above procedure without the addition of $Ni(NO_3)_2{\cdot}6H_2O$.

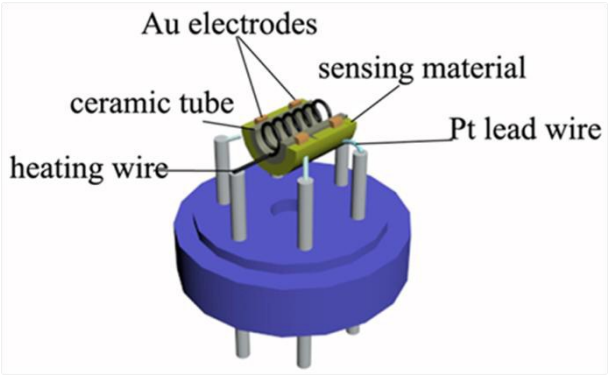

Figure 1. Schematic structure of the gas sensor

Characterization

Samples were characterized by X-ray diffraction(Rigaku D/MAX-2550 diffractometer, Cu-Kα radiation), nitrogen physisorption(Micromeritics Gemini VII surface area and porosity system at 77 K; samples degassed at 120 °C for 15 h), transmission electron microscopy(JEOL TEM-3010 instrument at an acceleration voltage of 200 kV). The specific surface area was computed with the five point Brunauer–Emmett–Teller(BET) method and the pore size distribution was obtained from the adsorption branch of the isotherms using the Barrett–Joyner–Halenda(BJH) analysis. Analysis of the X-ray photoelectron spectroscopy (XPS) was performed on Thermo ESCALAB 250 spectrometer. The morphology of the sample was recorded by field emission scanning electron microscopy(FESEM) using a JEOL JSM-7500F microscope, which was operated at 15 kV.

Sensor fabrication and measurement

For sensor fabrication, 50 mg of the as-prepared powder was dispersed in 0.5 mL deionized water to form paste which was deposited onto alumina ceramic tube. The length of alumina ceramic is 4 mm, external diameter is 1.2 mm, and internal diameter is 0.8 mm. The ceramic tube had a pair of Au electrodes with Pt lead wires which were used to be connected to the measure system. Then, the devices were dried under IR radiation for 1 h, sintered at 400 °C for 2 h and a Ni–Cr heating wire was inserted into the tube to form an indirect-heated gas sensor as showed in Fig.1. The gas-sensing properties of the samples were measured under laboratory conditions (20% ± 10% RH, 25 ± 1°C) in an organic glass chamber (50L). The measurement was carried out as follows: a given amount of the tested gas was injected into the chamber and then the sensor was put into the chamber for the measurement of the sensing properties. The electrical properties of the sensor were recorded by a digitalmultimeter (Fluke 8846A). The sensor response is defined as $S = R_a/R_g$ (reducing gas) and $S = R_g/R_a$ (oxidizing gas). R_a means the resistance in air while R_g is the resistance in the target gas. The response and recovery time are defined as the time cost in achieving 90% of the total resistance change in the case of adsorption and desorption, respectively.

Results and discussion

Ordered mesoporous In_2O_3 and Ni-doped In_2O_3 had been synthesized via nanocasting method with indium and nickel nitrate salts as precursors and SBA-15 as hard template. Sensing properties based on ordered mesoporous In_2O_3 and Ni-doped In_2O_3 were measured, and sensing mechanism was discussed. Large specific surface area and doping Ni into In_2O_3 improved the sensing performance.

Structure and morphology of as-prepared materials

The low-angle X-ray diffraction (XRD) patterns of mesoporous In_2O_3, Ni-doped In_2O_3 and SBA-15 samples were shown in Fig.2. For mesoporous Ni-doped In_2O_3 and In_2O_3, compared to the small-angle XRD pattern of SBA-15, a diffraction peak in Fig.2 could be indexed as the (100)

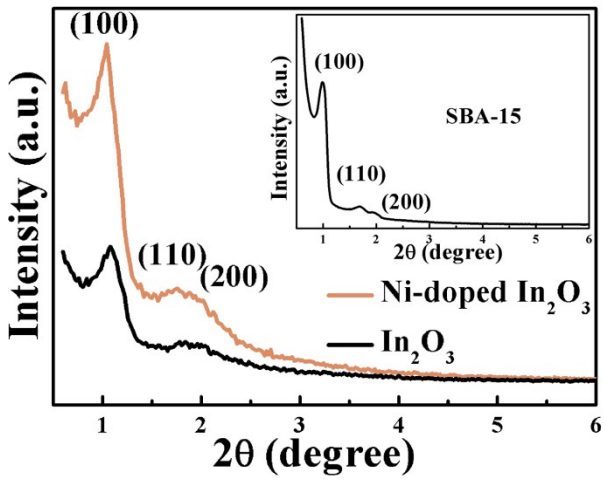

Figure 2. Low-angle XRD patterns of mesoporous In_2O_3, Ni-doped In_2O_3 and the hard template SBA-15(inset).

reflection clearly while (110), (200) diffraction peaks could be observed indistinctly. It means the samples are replicated from the template SBA-15 so that they have long-range order structure. However, the XRD peaks are somewhat broader than those in case of SBA-15, which indicates that the long-range order in the In_2O_3 and Ni-doped In_2O_3 samples is slightly lower.[32]

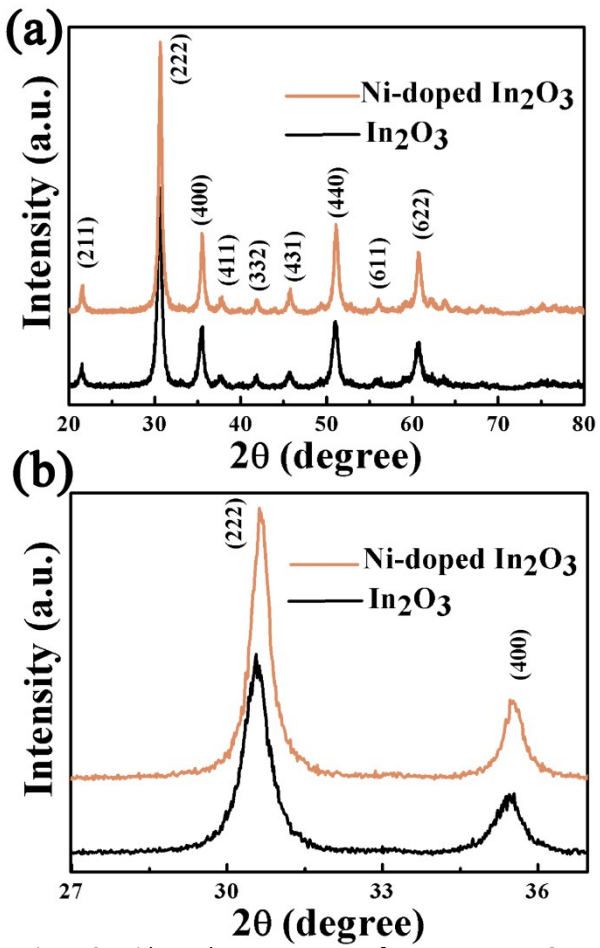

Figure 3. Wide-angle XRD patterns of mesoporous In_2O_3 and Ni-doped In_2O_3

Fig.3 showed the XRD patterns of the synthesized mesoporous undoped and Ni-doped In_2O_3. All the diffraction peaks could be indexed to the body-centered cubic In_2O_3 (JCPDS No. 06-0416). For the samples, no impure phases corresponding to Ni compounds were detected, which was probably due to the low content of Ni-dopant(0.46wt% by ICP-MS elemental analysis). Besides, it also can be attributed that Ni was effectively inserted into the crystal In_2O_3 lattice and stable Ni-doped In_2O_3 solid solution was formed. It could be seen that the (222) diffraction peak of Ni-doped In_2O_3 slightly shifted to the higher angles compared with that of In_2O_3 and further enlarged as shown in Fig.3(b).The lattice parameters of the mesoporous In_2O_3 and Ni-In_2O_3 were calculated to be 1.011 and 1.009 nm respectively, which was in accordance with the truth that the ionic radius of Ni^{2+} was smaller than that of In^{3+}. Furthermore, the colour of the prepared Ni-doped In_2O_3 had a soil yellow colour which was very different from the yellow colour of undoped In_2O_3. It also indicated the existence of Ni in the sample.[33] The resistance of Ni-doped In_2O_3 (3000 KΩ) was 60 times as high as that of undoped In_2O_3 (50 KΩ) at 58°C. The increase of resistance could be due to the substitution of In^{3+} ions with Ni^{2+} ions in cationic sites of In_2O_3 lattice. The crystallite size of samples can be calculated by the Scherrer equation,[23]

$$D = 0.9\lambda/(\beta \cos\theta) \quad (1)$$

where D is the crystallite size, λ is the wavelength of X-ray

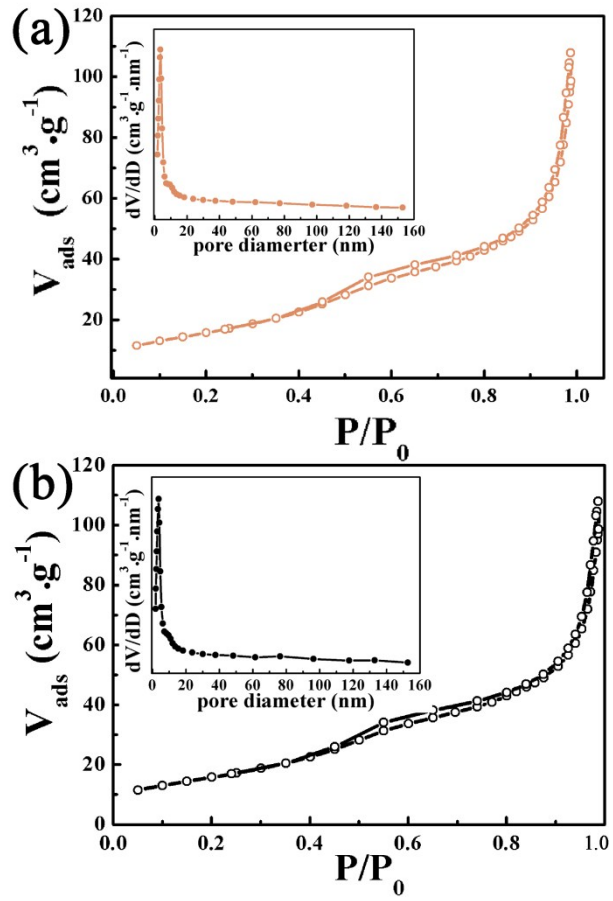

Figure 4. Nitrogen adsorption–desorption isotherms and corresponding pore size distribution(inset) of mesoporous Ni-doped In_2O_3(a) and In_2O_3(b) .

Table.1 The surface area, pore size and pore volume of mesoporous Ni-doped In_2O_3, undoped In_2O_3 and SBA-15

Sample	Surface area (m^2/g)	Pore size (nm)	Pore volume (cm^3/g)
Ni-doped In_2O_3	58.5	3.6	0.17
In_2O_3	50.3	3.2	0.15
SBA-15	394.2	7.2	0.59

radiation, β is the full width at half-maximum intensity (fwhm in radians), θ is diffraction angle. The average crystallite size of the mesoporous In_2O_3 and Ni-doped In_2O_3 are approximately 14.6 nm and 19.9 nm, respectively.

The nitrogen adsorption–desorption isotherms and the corresponding pore size distribution of mesoporous Ni-doped In_2O_3 and In_2O_3 were shown in Fig.4. The isotherms presented the typical type IV shape with H1 hysteresis loops, which indicated that the obtained In_2O_3 and Ni-doped In_2O_3 samples exhibited the mesoporous structure. The BET surface area, pore volume and pore size distribution of the template SBA-15, mesoporous In_2O_3 and Ni-doped In_2O_3 were listed in Table 1. Moreover, the surface area, nitrogen adsorption–desorption isotherms and corresponding pore size distribution of Ni-doped In_2O_3 without SBA-15 were mentioned in Supporting Information (Figure S1). The surface area of Ni-doped In_2O_3 without SBA-15(17.1 m^2/g) was much smaller than that of ordered mesoporous Ni-doped In_2O_3(58.3 m^2/g). It meant the nanocasting method using SBA-15 as template enhanced the surface area.

Detailed study about the structure of mesoporous Ni-doped In_2O_3 and undoped In_2O_3 were displayed in Fig.5(a),(c)

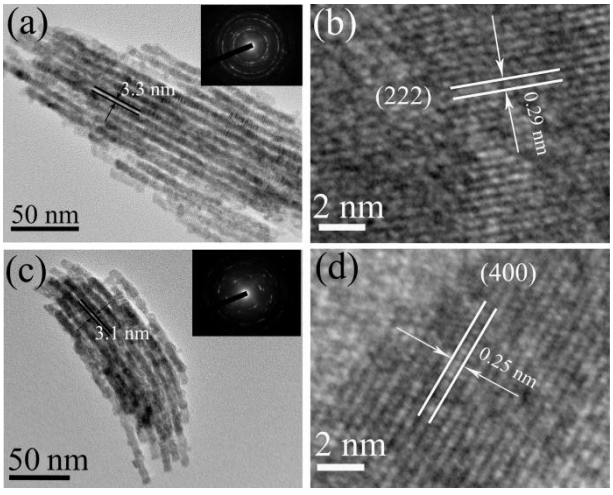

Figure 5. (a) Low resolution TEM micrographs of mesoporous Ni-doped In_2O_3 and SAED pattern (inset); (b)HRTEM micrograph showing enlarged lattice image of mesoporous Ni-doped In_2O_3; (c) Low resolution TEM micrographs of mesoporous undoped In_2O_3 and SAED pattern (inset); (d)HRTEM micrograph showing enlarged lattice image.

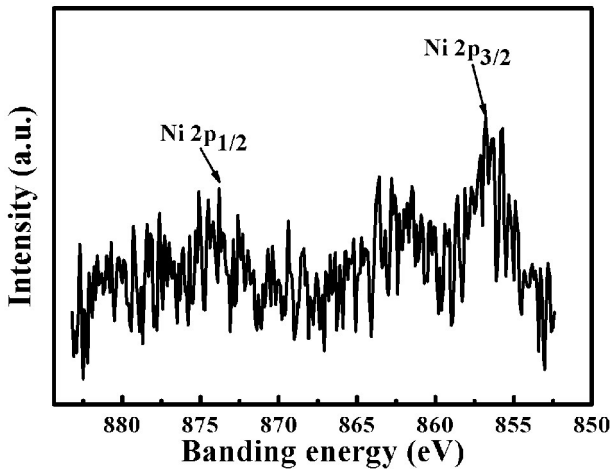

Figure 6. XPS spectrum in the Ni 2p region of the mesoporous Ni-doped In_2O_3

in which distinguishable periodic ordered mesostructure could be observed. It indicated that the samples had replicated from the silica templates. Besides, the sizes of pore of Ni-doped In_2O_3 and undoped In_2O_3 were 3.3 nm and 3.1 nm respectively, which was identical with those in Table 1. The selected-area electron diffraction (SAED) patterns of mesoporous Ni-doped and undoped In_2O_3 (Fig. 5(a), (c) inset) showed that the samples were polycrystalline in structure. Fig.5(b) showed fringe distance of 0.29 nm which was corresponding to the crystal planes (222) planes. Similarly, Fig.5(d) showed fringe distance of 0.25 nm which was corresponding to the crystal planes (400). Furthermore, to investigate the morphology of mesoporous Ni-doped In_2O_3, the SEM patterns of ordered mesoporous Ni-doped In_2O_3 was provided in Supporting Information (Figure S2).

To further investigate the valence of Ni-dopant, XPS data was collected and presented in Fig.6. Fig.6 showed weak signals at 856.5eV and 873.8eV for Ni $2p_{3/2}$ and Ni $2p_{1/2}$, which could be ascribed to the Ni^{2+} respectively. The weak peaks around 862.0 and 880.0eV were due to the shakeup satellite structures of Ni $2p_{3/2}$ and Ni $2p_{1/2}$.[33, 34]

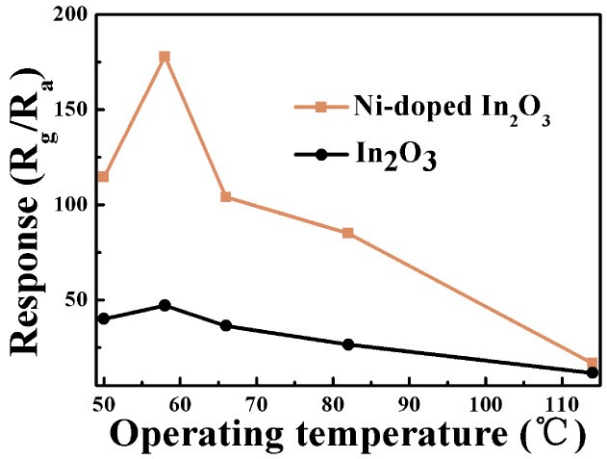

Figure 7. Responses of undoped In_2O_3 and Ni-doped In_2O_3 to 500ppb NO_2 at different operating temperatures.

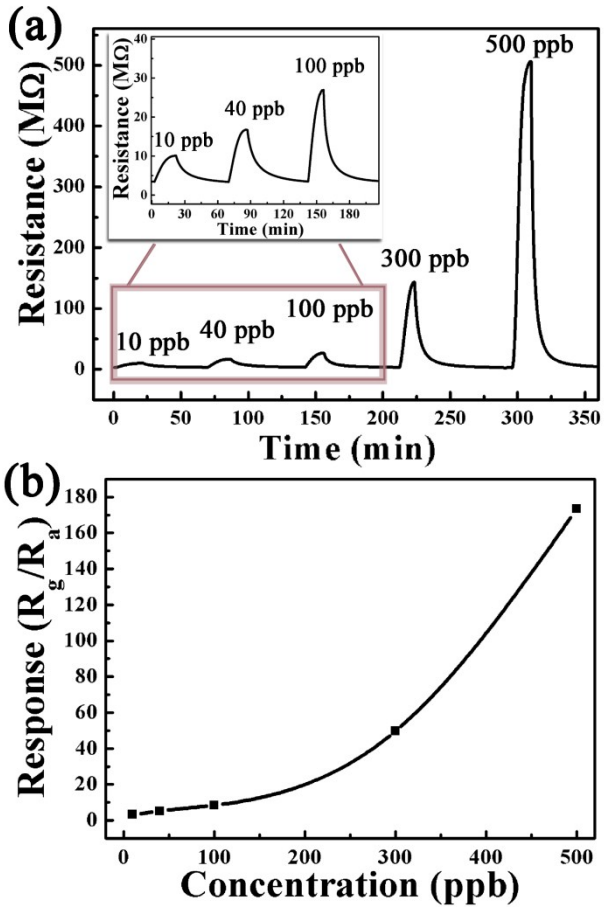

Figure 8.(a) Response and recovery characteristics of the sensor based on Ni-doped In_2O_3;(b) response of the sensor based on Ni-doped In_2O_3 to various concentrations of NO_2 at 58°C.

Sensing properties

The response of the sensors based on In_2O_3 and Ni-doped In_2O_3 to 500 ppb NO_2 were measured under different operating temperatures to investigate the optimal operating temperature. The results were shown in Fig.7 and the sensor based on Ni-doped In_2O_3 had extremely high response (178) at the relatively low temperature (58°C), which was nearly 4 times higher than that of undoped In_2O_3 (49).

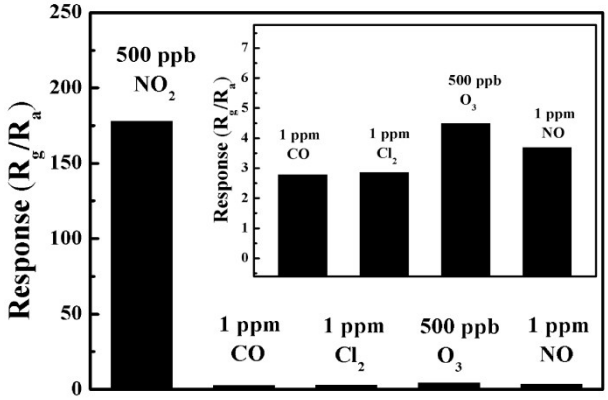

Figure 9.Responses of mesoporous Ni-doped In_2O_3 to different gases at 58°C

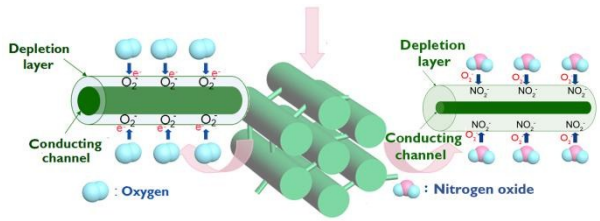

Figure 10.Schematic illustration of the NO_2 sensing mechanism of In_2O_3 sensor

The dynamic response performances of the sensor based on mesoporous Ni-doped In_2O_3 to NO_2 was investigated at the operating temperature of 58°C under different concentration of NO_2. The response time was about 9 min to 500 ppb NO_2. In Fig.8(a), it could be observed that when the sensor was exposed to various concentration of NO_2, it could reach obvious response even to 10 ppb NO_2 (In Fig.8(b), it reached 3.). And then when the sensor was exposed to the air, the resistance decreased back to the baseline in each circle. It suggested that its good stability with no observation of baseline shift in several detection cycles. In Fig.8(b), the sensor displayed higher response with the increased in concentration of NO_2. This suggested that the sensor based on mesoporous Ni-doped In_2O_3 was favorable to detect NO_2 with low concentration.

Selectivity was one of the important parameter for the gas sensors. The responses of the sensor to various testing gases at the operating temperature of 58°C were tested including NO, O_3, CO, Cl_2 in order to investigate the selectivity of the sensor based on mesoporous Ni-doped In_2O_3. It was obvious that the sensor exhibited the significant response towards 500 ppb NO_2 against other gases (1 ppm CO, 1 ppm Cl_2, 1 ppm NO, 500 ppb O_3). Such a result indicated that the mesoporous Ni-doped In_2O_3 sensor exhibited an excellent selectivity towards NO_2 against the other tested gases at 58°C.

The gas-sensing mechanism of n-type semiconductor sensor has been discussed in early literature.[34] It is based on the change of electrical conductivity at adsorption and desorption of gas molecules on the surface of sensing materials. When mesoporous Ni-doped In_2O_3 sensor is exposed in air, the adsorbed oxygen molecules capture electrons from the semiconductor oxide so that chemical adsorption oxygen species (O_2^-, O^- and O^{2-}) are generated. The chemisorbed oxygen species result in the formation of a depletion layer at grain boundaries. When mesoporous Ni-doped In_2O_3 sensor is exposed to NO_2 gas, the NO_2 molecules contact with and then physically adsorb onto the surface of In_2O_3. Then, NO_2 molecules can not only capture electrons from the conduction band but also react with the adsorbed oxygen species as shown in Fig.10: [23]

$NO_2(gas)+e^- \rightarrow NO_2^-(ads)$ (2)

$NO_2(gas)+O_2^-(ads)+2e^- \rightarrow NO_2^-(ads)+2O^-(ads)$ (3)

Besides, The incorporation of Ni acts as an acceptor-type impurity so that it can increase the number of oxygen vacancies based on solid state chemistry theory.[36] And oxygen vacancies which are very important to the adsorption of oxygen on the surface of sensing materials are beneficial to enhance the response.[35-37] It suggests that sensor response is

Table 2. Gas sensing performances based on different materials

Materials	Concen-tration	Operating temperature	Response (R_g/R_a)	References
Corundum In_2O_3	1ppm	250	2.0	38
TeO_2/CuO	500ppb	150	2.2	39
GaN/WO_3	1ppm	300	2.2	40
CuO-ZnO	10ppm	300	0.5	41
This study	10ppb	58	3	This study

improved due to nickel presence and the additive plays an important role in the interaction between the semiconductor oxide and the target gas. Furthermore, higher surface area can provide more active sites to interact with NO_2, which is also attributed to the high response. And the structure of mesoporous In_2O_3 also facilitates the adsorption of NO_2.[23] All the factors are obviously beneficial for higher response and low detection limit. Table 2 showed NO_2 sensing performances based on different materials under rather low concentration. The response of the mesoporous Ni-doped In_2O_3 is higher than those of others. Besides, compared to other materials[38, 39, 40, 41] the operating temperature is very low. Obviously, the sensor based on mesoporous Ni-doped In_2O_3 can detect lower concentration of NO_2 at lower temperature.

Conclusions

In conclusion, the mesoporous undoped and Ni-doped In_2O_3 had been synthesized by a nanocasting method. The results of characterization showed that both Ni-doped and undoped In_2O_3 had long-range order mesoporous structure with large specific surface area. The patterns of TEM and nitrogen physisorption showed the pore sizes were around 3 nm. Besides, the response of the sensor based on mesoporous Ni-doped In_2O_3 to 500 ppb NO_2 was nearly four times higher that of mesoporous undoped In_2O_3. Moreover, the sensor based on mesoporous Ni-doped In_2O_3 had very low detection limit to 10 ppb NO_2. It seemed that Ni-doping may improve the formation of surface oxygen vacancy, which was probably responsible for the enhanced performance.

Acknowledgements

This work was supported by the National Nature Science Foundation of China (61134010, 61304242, 61327804, 61377058 and 61374218), Program for Chang Jiang Scholars and Innovative Research Team in University (No.IRT13018), National High-Tech Research and Development Program of China (863 Program, No. 2013AA030902 and 2014AA06A505), China Postdoctoral Science Foundation (No.2013M530979), Science and Technology Development Program of Jilin Province(No.20150520091JH).

Notes and references

1 Q. Diao, C. Yin, Y. Guan, X. Liang, S. Wang, Y. Liu, Y. Hu, H. Chen and G. Lu, *Sensors and Actuators B-Chemical*, 2013, 177, 397-403.
2 J. Kong, N. R. Franklin, C. W. Zhou, M. G. Chapline, S. Peng, K. J. Cho and H. J. Dai, *Science*, 2000, 287, 622-625.
3 N. Yamazoe, G. Sakai and K. Shimanoe, *Catalysis Surveys from Asia*, 2003, 7, 63-75.
4 A. Shanmugasundaram, P. Basak, S. V. Manorama, B. Krishna and S. Sanyadanam, *ACS applied materials & interfaces*, 2015, 7, 7679-7689.
5 A. Shanmugasundaram, B. Ramireddy, P. Basak, S. V. Manorama and S. Srinath, *The Journal of Physical Chemistry C*, 2014, 118, 6909-6921.
6 T. Waitz, T. Wagner, T. Sauerwald, C. D. Kohl and M. Tiemann, *Advanced Functional Materials,*2009, 19, 653-661.
7 H. Shan, C. B. Liu, L. Liu, J. B. Zhang, H. Y. Li, Z. Liu, X. B. Zhang, X. Q. Bo and X. Chi, *ACS applied materials & interfaces*, 2013, 5, 6376-6380.
8 S. L. Bai, S. Chen, Y. B. Zhao, T. Guo, R. X. Luo, D. Q. Li and A. F. Chen, *Journal of Materials Chemistry A*, 2014, 2, 16697-16706.
9 Z. Wang, P. Sun, T. Yang, Y. Gao, X. Li, G. Lu and Y. Du, *Sensors and Actuators B-Chemical*, 2013, 186, 734-740.
10 10.S. L. Bai, S. Chen, L. Y. Chen, K. W. Zhang, R. X. Luo, D. Q. Li and C. C. Liu, *Sensors and Actuators B-Chemical*, 2012, 174, 51-58.
11 11.H. L. Cai, B. Liu, Q. A. Qiao and Z. D. Lin, *Nanosci Nanotech Let*, 2014, 6, 701-705.
12 Y. Shimizu and M. Egashira, *Mrs Bulletin*, 1999, 24, 18-24.
13 S. D. Choi and B. K. Min, *Sensors and Actuators B-Chemical*, 2001, 77, 330-334.
14 J. H. Lee, *Sensors and Actuators B-Chemical*, 2009, 140, 319-336.
15 X. L. Hu, X. Zhou, B. Wang, P. Sun, X. W. Li, C. Wang, J. Y. Liu and G. Y. Lu, *Rsc Adv*, 2015, 5, 4609-4614.
16 A. K. Jana, *J Photoch Photobio A*, 2000, 132, 1-17.
17 N. K. Singh and A. Mondal, *J Nanosci Nanotechno*, 2015, 15, 6098-6102.
18 M. Ali, C. Y. Wang, C. C. Roehlig, V. Cimalla, T. Stauden and O. Ambacher, *Sensors and Actuators B-Chemical*, 2008, 129, 467-472.
19 X. Xu, X. Mei, P. Zhao, P. Sun, Y. Sun, X. Hu and G. Lu, *Sensors and Actuators B: Chemical*, 2013, 186, 61-66.
20 J. Zhao, T. L. Yang, Y. P. Liu, Z. Y. Wang, X. W. Li, Y. F. Sun, Y. Du, Y. C. Li and G. Y. Lu, *Sensors and Actuators B-Chemical*, 2014, 191, 806-812.
21 P. F. Guo and H. B. Pan, *Sensors and Actuators B-Chemical*, 2006, 114, 762-767.
22 P. Li, H. Q. Fan, Y. Cai and M. M. Xu, *Crystengcomm*, 2014, 16, 2715-2722.
23 J. Zhao, T. Yang, Y. Liu, Z. Wang, X. Li, Y. Sun, Y. Du, Y. Li and G. Lu, *Sensors and Actuators B: Chemical*, 2014, 191, 806-812.
24 Y. Chen, L. Zhu, C. Feng, J. Liu, C. Li, S. Wen and S. Ruan, *Journal of Alloys and Compounds*, 2013, 581, 653-658.
25 M. W. Ahn, K. S. Park, J. H. Heo, J. G. Park, D. W. Kim, K. J. Choi, J. H. Lee and S. H. Hong, *Applied Physics Letters*, 2008, 93.
26 A. Z. Sadek, S. Choopun, W. Wlodarski, S. J. Ippolito, K. Kalantar-zadeh, IEEE SENSORS JOURNAL, 2007. 7
27 C. J. Chang, J. K. Chen and T. L. Yang, *J. Taiwan Inst. Chem. Eng.*, 2014, 45, 1876-1882.
28 X.-D. Wang, Y.-L. Wang, Y. Chen, C. Si, A. Su and D.-J. Lee, *Journal of the Taiwan Institute of Chemical Engineers*, 2014, 45, 1532-1541.
29 C.-J. Chang, C.-Y. Lin, J.-K. Chen and M.-H. Hsu, Ceramics International, 2014, 40, 10867-10875..
30 A. Yu, J. Qian, H. Pan, Y. Cui, M. Xu, L. Tu, Q. Chai and X. Zhou, *Sensors and Actuators B-Chemical*, 2011, 158, 9-16.
31 C. J. Chang, C. K. Lin, C. C. Chen, C. Y. Chen and E. H. Kuo, *Thin Solid Films*, 2011, 520, 1546-1553.

32 E. Rossinyol, A. Prim, E. Pellicer, J. Arbiol, F. Hernandez - Ramirez, F. Peiro, A. Cornet, J. R. Morante, L. A. Solovyov, B. Tian, T. Bo and D. Zhao, *Advanced Functional Materials*, 2007, 17, 1801-1806.

33 X. Liu, J. Zhang, X. Guo, S. Wu and S. Wang, *Sensors and Actuators B: Chemical*, 2011, 152, 162-167.

34 K. Wetchakun, T. Samerjai, N. Tamaekong, C. Liewhiran, C. Siriwong, V. Kruefu, A. Wisitsoraat, A. Tuantranont and S. Phanichphant, *Sensors and Actuators B: Chemical*, 2011, 160, 580-591.

35 P. Sun, X. Zhou, C. Wang, B. Wang, X. Xu and G. Lu, *Sensors and Actuators B: Chemical*, 2014, 190, 32-39.

36 D. Wang, J. Sun, X. Cao, Y. Zhu, Q. Wang, G. Wang, Y. Han, G. Lu, G. Pang and S. Feng, *Journal of Materials Chemistry A*, 2013, 1, 8653.

37 P. Bogdanov, M. Ivanovskaya, E. Comini, G. Faglia and G. Sberveglieri, *Sensors and Actuators B: Chemical*, 1999, 57, 153-158.

38 L. Gao, Z. Cheng, Q. Xiang, Y. Zhang and J. Xu, *Sensors and Actuators B-Chemical*, 2015, 208, 436-443.

39 S. Park, S. Kim, G.-J. Sun, W. I. Lee, K. K. Kim and C. Lee, *Nanoscale Research Letters*, 2014, 9.

40 S. Park, H. Ko, S. Kim and C. Lee, *Ceramics International*, 2014, 40, 8305-8310.

41 C. Jin, H. Kim, S. Park, S.-W. Choi, S. S. Kim and C. Lee, *Surface and Interface Analysis*, 2012, 44, 1534-1537.

Table of Contents

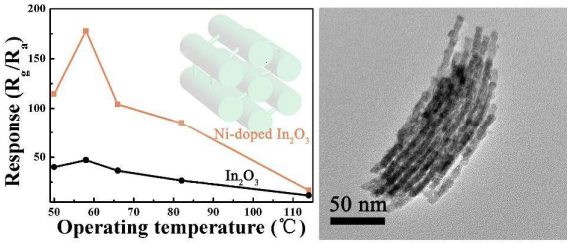

This study demonstrated that doping Ni enhanced the response of the sensor based on mesoporous In_2O_3 to NO_2.